Quantifying reaction spread and x-ray exposure sensitivity in hydrogen silsesquioxane latent resist patterns with x-ray spectromicroscopy

Allison G. Caster,[a] Stefan Kowarik,[b] Adam M. Schwartzberg,[c] and Stephen R. Leone[d]
Chemical Sciences Division, Lawrence Berkeley National Laboratory, Berkeley, California 94720 and Department of Chemistry and Department of Physics, University of California, Berkeley, California 94720

Alexei Tivanski[e] and Mary K. Gilles
Chemical Sciences Division, Lawrence Berkeley National Laboratory, Berkeley, California 94720

(Received 8 June 2010; accepted 18 October 2010; published 29 November 2010)

Direct-write soft x-ray lithography with an ~50 nm diameter beam is used to pattern features in hydrogen silsesquioxane (HSQ) thin films. Scanning transmission x-ray microscopy of the undeveloped patterns (latent patterns) at the oxygen *K*-edge reveals a two-stage cross-linking mechanism. Oxygen and silicon near edge x-ray absorption fine structure spectra of latent patterns show an increase in oxygen content and no change in silicon content within exposed regions. A dose and thickness dependent spatial spread of the cross-linking reaction beyond the exposure boundaries is observed and quantified in detail. Strong area-dependent exposure sensitivity (attributed to cross-linking beyond the exposed region) is observed in latent patterns. A lateral spread in the cross-linking of >70 nm (full width at half maximum) is observed on both sides of the lines created with 580 eV x-rays ($\lambda = 2.14$ nm) in 330 ± 50 nm thick HSQ films at low dose (0.6 ± 0.3 MGy, 27 ± 12 mJ/cm^2) (1 MGy$=10^6$ J/kg absorbed energy). At a higher dose (111 ± 29 MGy, 5143 ± 1027 mJ/cm^2), this spread increased to 150 nm. Preliminary results indicate that latent line widths increased with increasing delay between film spin-coating and exposure. Sharper lines are observed after room temperature development of the latent HSQ patterns in NaOH/NaCl solution (onset dose of 3.9 ± 1.0 MGy, 181 ± 36 mJ/cm^2) due to the removal of material below a critical degree of cross-linking. Given the short range of low energy secondary electrons in condensed media (<10 nm at ≤580 eV), the observed spread is likely due to the propagation of reactive ions or radicals beyond the exposed regions. © *2010 American Vacuum Society.*
[DOI: 10.1116/1.3514124]

I. INTRODUCTION

The negative-tone photoresist hydrogen silsesquioxane (HSQ) is a promising material for sub-20-nm electron beam (e-beam) lithography and photolithography because of its small molecular size, low dielectric constant, and excellent mechanical stability.[1,2] However, a better understanding of the cross-linking chemistry is necessary to utilize HSQ and its derivatives for commercial nanolithography. In research environments, e-beam lithography of HSQ produces high aspect-ratio, nanoscale features (as small as 4.5 nm; see Ref. 3) that are used for optical devices such as extreme ultraviolet (EUV) diffraction gratings,[4] x-ray zone plates,[5–7] and nanoantennas for optical field enhancement,[8] as well as high-density line patterns for the next generation of integrated circuits and computer memory.[9,10] Often, the exposure dose and developer conditions required to achieve the desired feature size and contrast are unpredictable.[1,11,12] Irreproducibility in the features is caused by sample quality and age,[13] time delay effects,[13,14] and area-dependent sensitivity.[4,15–17] Therefore, recent studies have focused on determining the optimum parameters for producing the smallest features via e-beam lithography of HSQ,[3,11,15,18] but many questions remain unanswered.[1]

While e-beam lithography is an important patterning modality for HSQ, commercial integrated circuit manufacturing requires high-throughput optical lithography. EUV interference lithography of HSQ has been used to form dense line patterns (20 nm half-pitch),[19] and x-ray exposure behind a mask has created isolated 11 nm wide features in 50 nm thick HSQ films.[20,21] This line width resolution surpasses that of conventional chemically amplified resists,[9] but with insufficient sensitivity and reproducibility for high-throughput commercial applications. To address these issues, new and improved HSQ derivatives and similar materials are under development.[22] Progress could be hastened by understanding the fundamental chemistry that creates the current challenges with HSQ.

HSQ, a cagelike molecule with the formula $H_8Si_8O_{12}$, belongs to the class of compounds known as polyhedral oligomeric silsesquioxanes. Also known as "spin-on glass" and

[a]Present address: Department of Bioengineering, University of Colorado Denver, Aurora, CO 80045.
[b]Present address: Department of Physics, Humboldt Universität zu Berlin, Germany.
[c]Present address: Sandia National Laboratories, Livermore, CA, 94551.
[d]On appointment as a Miller Research Professor in the Miller Institute for Basic Research in Science; electronic addresses: srl@berkeley.edu and srl@cchem.berkeley.edu
[e]Present address: Department of Chemistry, University of Iowa, Iowa City, IA 52242.

Author complimentary copy. Redistribution subject to AIP license or copyright, see http://jvb.aip.org/jvb/copyright.jsp

developed as an interlayer dielectric film for integrated circuits,[23,24] extremely thin HSQ films are applied from a volatile solution via spin-coating, then cross-linked to an insoluble, glasslike SiO_2 network structure via heat,[25] e-beam,[2,15,17] proton beam,[26] He^+ beam,[27] ultrafast pulses of near IR light,[28,29] EUV radiation, or x-ray exposure.[30–32] After cross-linking, the unexposed HSQ is selectively dissolved by a basic or organic developer solution.[1] In most studies, scanning electron microscopy (SEM) or atomic force microscopy imaging of the patterns is performed after e-beam exposure and development. One drawback of such post-development analysis is that the chemical effects of exposure are coupled with the development chemistry, and the features produced are sensitive to changes in the development process.[12,15,33,34] To address questions pertaining solely to the exposure-induced chemical changes, undeveloped (latent) photoresist patterns can be imaged at high spatial resolution (~30 nm) with scanning transmission x-ray microscopy (STXM).[16,35] Differences in bonding structure around the Si and O atoms in HSQ before and after cross-linking are measured using near edge x-ray absorption fine structure (NEXAFS) spectroscopy. These changes in bonding reflect the degree of cross-linking in the exposed versus unexposed regions of the HSQ film prior to development. A previous STXM study on latent HSQ patterns reported bonding changes extending up to 12 μm beyond the exposure boundaries at high e-beam doses (approximately 50 mC/cm^2 in a 250 nm thick film).[16]

Here, NEXAFS spectroscopy and STXM imaging of x-ray exposed HSQ are used to quantify the range of the reaction spread, cross-linking rate, and x-ray exposure sensitivity of HSQ in the absence of development effects. We observe a two-stage x-ray induced cross-linking process resulting in the incorporation of additional oxygen atoms into the cross-linked regions. The full width at half maximum (FWHM) spread of the cross-linking reaction is >70 nm, depending on the film thickness and x-ray dose. The reaction spread results in proximity effects, including significant area-dependent sensitivity. Comparing the patterns before and after development shows that a partially cross-linked material is removed by the NaOH/NaCl developer, including regions cross-linked by reaction spread. Thus, the underlying causes of the proximity effects are not fully apparent after development.

II. EXPERIMENT

HSQ thin films, 100–500 nm thick, are prepared on 100 nm thick silicon nitride substrates. For patterning, spectroscopy, and imaging, the sample patterns are written and analyzed in the STXM at beamline 5.3.2 at the Advanced Light Source (ALS), Lawrence Berkeley National Laboratory, Berkeley, CA.[36] For lithography, x-rays at 536 or 580 eV are tightly focused on the film surface to an approximately 50 nm diameter spot (FWHM), and the sample is raster scanned through the x-ray beam in a predefined pattern. Oxygen *K*-edge NEXAFS spectra (520–700 eV) allow the assessment of changes in the chemical structure surrounding the oxygen atoms before and after x-ray exposure. Within 5 min of patterning, images of exposed patterns are measured with ~30 nm spatial resolution; additional cross-linking is minimized with reduced photon flux and rapid scanning at a single fixed energy (536 eV, oxygen *K*-edge). Analysis of these images measures the relative degree of chemical change for each set of conditions. Corresponding NEXAFS spectra at the silicon atom *K*-edge (1825–1880 eV) are measured on beamline 11.0.2 of the ALS.[37]

A. Sample preparation

To prepare HSQ films, 5 μl of Dow Corning XR-1541 (for 100 nm thick films), Dow Corning FOx-15® (300–400 nm thickness), or Dow Corning FOx-25® (500 nm thickness) are spin-cast at 2000–6000 rpm for 30 s onto a 100 nm thick silicon nitride (Si_3N_4) membrane substrate (Silson Limited). Periodically, the transmitted spectrum and photon flux through a blank substrate are measured to obtain the background (necessary to convert the signal to absorbance). HSQ stock solutions were stored continuously at −15 °C for up to 2.5 years. Previous reports suggest that contrast and sensitivity depend on how recently the HSQ was synthesized, but that the effect of a delay between prebake and exposure is greater.[13] Only films noted as "prebaked" were baked on a hot plate in air for 5 min at 150 °C to remove excess solvent prior to exposure. To aid in focusing, a 1.5 μl droplet of dilute, 100 nm gold nanoparticles is pipetted onto the surface. The films are then stored in air for ~15 h prior to exposure and imaging in the x-ray microscope. The microscope chamber is evacuated to 0.2 Torr (~26.7 Pa) then backfilled with 300 Torr of He.

B. STXM lithography and imaging

The STXM at beamline 5.3.2 uses a Fresnel zone plate lens (25 nm outer diameter) to focus synchrotron-generated soft x-rays to a 30–50 nm diameter spot. By focusing on a 100 nm nanoparticle on the sample surface,[36] the beam is tightly focused through the entire film thickness (≤500 nm). A monochromator selects the photon energy with <0.1 eV spectral resolution. The monochromator entrance slit, plus vertical and horizontal exit slits, controls the spectral and spatial resolution of the microscope and photon flux.[36] For patterning, wide settings for the three slits (80, 40, and 40 μm) yield a photon flux on the order of 10^6 photons/s with an ~50 nm beam diameter (FWHM). For imaging, narrow slits (40, 20, and 20 μm) reduce the photon flux by a factor of ~4 and improve the spatial resolution to ~30 nm.[38]

To obtain images at a fixed energy, the x-ray transmission is measured as the sample is raster scanned through the focal point. For NEXAFS spectra, the photon energy is scanned for each point of interest. The transmitted signal is compared to that through a blank silicon nitride membrane substrate and converted to optical density (OD) according to the following equation:

Author complimentary copy. Redistribution subject to AIP license or copyright, see http://jvb.aip.org/jvb/copyright.jsp

$$\mathrm{OD} = -\ln\left(\frac{I}{I_0}\right) = \mu(E)\rho l, \quad (1)$$

where I is the x-ray flux through the sample plus substrate and I_0 is the photon flux through the blank substrate, and the natural logarithm form is used. The measured OD is sensitive to the sample thickness, l, density, ρ, and energy-dependent mass absorption coefficient, $\mu(E)$. At the oxygen K-edge, a minimum HSQ film thickness of ~300 nm was used to obtain high signal-to-noise ratios. The contrast within each image, which is related to the degree of cross-linking, is quantified by calculating the relative OD (ΔOD) between exposed and unexposed regions as follows:

$$\Delta\mathrm{OD} = |\mathrm{OD}_{\mathrm{exposed}} - \mathrm{OD}_{\mathrm{unexposed}}| = \left| -\ln\left(\frac{I_{\mathrm{exposed}}}{I_0}\right) + \ln\left(\frac{I_{\mathrm{unexposed}}}{I_0}\right) \right| = \left| -\ln\left(\frac{I_{\mathrm{exposed}}}{I_{\mathrm{unexposed}}}\right) \right|. \quad (2)$$

An approximately Gaussian beam profile is assumed, with a 50 nm FWHM and extended tail, based on the measured spatial resolution and previously reported knife-edge measurements.[39,40] For single-pass lines, the sample is scanned through the focal point with a fixed step size of 50 nm or 200 nm and an exposure time (dwell time) from 2 ms to 7.7 s per pixel. Longer dwell times or smaller step sizes result in a higher deposited dose and, thus, a greater degree of cross-linking. Wide features are patterned by exposing n adjacent single-pass lines, with the space between lines equal to the step size (50 nm or 200 nm). See supplementary material in Ref. 41 for detailed beam profile and exposure patterns.

HSQ x-ray patterning near the oxygen K-edge involves a resonant or near-resonant absorption. The absorbed dose is calculated by

$$a = FEt/m\varepsilon, \quad (3)$$

where a is the absorbed radiation in units of megagrays (MGy) (1 MGy$=10^6$ J kg^{-1}), F is the flux absorbed (photons/s) at energy E in exposure time t of a specific irradiated volume of the HSQ with mass m, and ε is the photon counting efficiency of the detector at energy E ($57\pm5\%$ at 536 eV).[36,42] The mass is calculated from the irradiated area, sample thickness, and density. The density for non-cross-linked HSQ is assumed to be 1.3–1.5 g/cm^3.[43] The film thickness is estimated for each patterned region by fitting the oxygen K-edge NEXAFS spectrum to that calculated per nanometer thickness of HSQ.[44–46] The uncertainty in each quantity in Eq. (3) is propagated for all dose values.

At 580 eV, the optical density changes very little with exposure time, and the absorbed flux, F, is taken as the difference between the flux through the blank substrate (I_0) and the flux through the unexposed sample (I),

$$F = I_0 - I. \quad (4)$$

However, at 536 eV the OD changes with exposure time, and absorbed flux is calculated according to

$$F = I_0[1 - \exp(-\mathrm{OD}(t))], \quad (5)$$

where empirical data are used to fit the OD versus exposure time. For ease of comparison to dose values in the literature for EUV lithography, the area dose is also calculated by

$$D = FEt/A\varepsilon, \quad (6)$$

where D is the absorbed radiation dose in units of mJ/cm^2, and A is the irradiated area; this does not account for differences in sample thickness.

Within 5 min of x-ray exposure, patterned regions are imaged at 536 eV at a higher spatial resolution (~30 nm) and reduced x-ray flux. For patterning, the slit width, dwell time, and step size result in a total dose of 0.4–300 MGy, while imaging settings are optimized for <0.1 MGy absorbed dose. No increase in STXM contrast was observed for regions with <0.1 MGy dose, confirming that little or no cross-linking occurs during imaging. After x-ray exposure and imaging, patterned films are developed for 4 min at room temperature in a high-contrast developer solution of 1 wt % NaOH and 4 wt % NaCl in Millipore water to remove any unexposed material.[47] The developed patterns are subsequently imaged again using STXM and a field emission scanning electron microscope (JEOL JSM 6340F).

III. RESULTS AND DISCUSSION

A. NEXAFS spectra of x-ray exposed HSQ

The oxygen K-edge NEXAFS spectrum of a prebaked, 525 ± 50 nm thick unexposed HSQ film, shown in Fig. 1(a), is obtained by defocusing the x-ray beam to a spot size of 20 μm (total dose ~0.02 ± 0.01 MGy). A small peak is observed at 536.1 ± 0.1 eV on the shoulder of a broader peak centered at ~538.8 eV. After focusing the x-ray beam, the spectrum is remeasured. This results in a total dose of 808 ± 213 MGy after the spectral acquisition (from 520 to 600 eV). As shown in the difference spectrum in Fig. 1(a), the additional exposure results in a pronounced decrease in OD at 535.9 ± 0.1 eV along with an increase in the broader peak (538.8 eV) and post-edge OD (for example, at 590 eV). Because the absorbed dose is cumulative, the exposure level increases slightly at each consecutive energy during the measurement of the "exposed" spectrum.

For comparison, the oxygen spectra in Fig. 1(b) are from a sequence of images as a function of energy, called an "image stack," which provides a spectrum at each image pixel.[36] A small region (0.5 μm^2) of an unbaked 300 ± 50 nm thick film is uniformly exposed to 47 ± 15 MGy at 580 eV. The image stack is subsequently acquired from this exposed region and the surrounding film, and the spectra shown are averaged over these two separate regions. (The image stack adds 3 ± 1 MGy of dose, inducing a small increase in cross-linking over both regions.) The NEXAFS peak positions in Fig. 1(b) agree within uncertainty to those in Fig. 1(a). Varia-

Author complimentary copy. Redistribution subject to AIP license or copyright, see http://jvb.aip.org/jvb/copyright.jsp

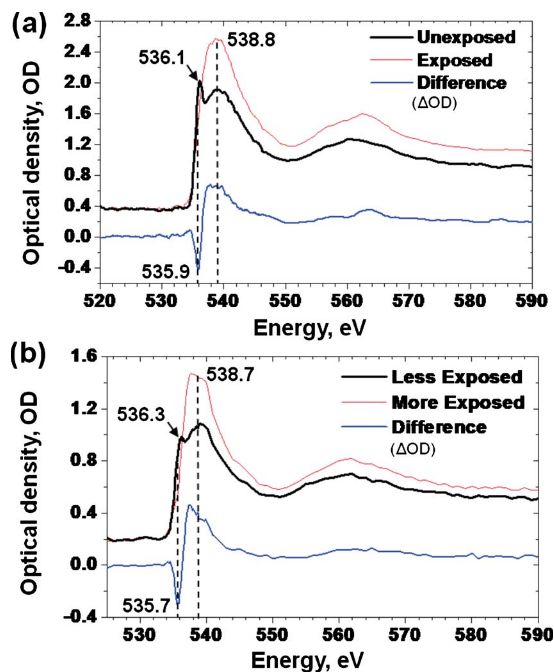

FIG. 1. (Color online) (a) Oxygen *K*-edge NEXAFS spectra of a HSQ thin film before (unexposed) and after (exposed) x-ray exposure (808 MGy, 520–600 eV). The differences are attributed to x-ray induced cross-linking and ~30% increase in total oxygen content. (b) Similar peak shifts and a smaller increase in oxygen content are observed for a smaller dose in a slightly thinner film. Less exposed=3 MGy, more exposed=50 MGy (580 eV).

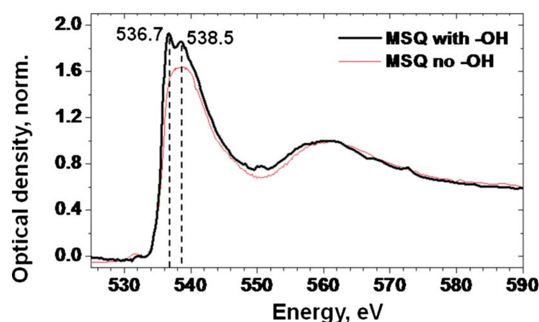

FIG. 2. (Color online) Oxygen *K*-edge NEXAFS spectra for pure MSQ with no ⋝Si–OH compared to MSQ with incorporated ⋝Si–OH, suggesting that the ~536 eV peak in Fig. 1 is likewise due to ⋝Si–OH in as-spun HSQ.

tions in line shape are attributed to differences between the two samples, including sample type, age, prebake conditions, and exposure parameters.

The oxygen *K*-edge NEXAFS spectra observed here are similar to those previously reported for unexposed versus e-beam cross-linked HSQ films.[16] The spectral modifications in HSQ after exposure are attributed to changes in bonding around the oxygen atoms due to x-ray induced polymer network formation (cross-linking). The broad absorption band at ~539 eV increases as the HSQ cross-links to a more SiO_2-like structure, due to an increase in the $1s \rightarrow \sigma^*$ (O–Si) absorption that occurs at this energy in SiO_2.[48,49] The broad band at ~562 eV, present before and after cross-linking, arises from a "shape resonance" of the same transition.[48–51]

Previously, the broad 539 eV peak was also assigned to adsorbed water multilayers on various surfaces.[52,53] Additionally, the NEXAFS spectra in Fig. 1(a) indicate that the total oxygen content within the exposed regions (808 MGy) increases by ~30% (evidenced by the increase in x-ray absorption beyond the oxygen edge, from 550 to 590 eV). For smaller doses [Fig. 1(b), 3 vs 50 MGy], a correspondingly smaller increase in oxygen content is observed. Hence, the oxygen content increases with increasing dose. This oxygen could be incorporated into the network during cross-linking or come from water adsorbed on the surface and within pores in cross-linked regions, possibly due to decreased hydrophobicity and altered pore size of the network structure.[25,43,54,55] At the lowest vacuum pressure used in the STXM chamber (0.2 Torr), many monolayers of water exist on the film surface and surfaces of the experimental chamber. Water is also mobile within the porous HSQ network (in cross-linked HSQ, diffusion coefficient of $H_2O \approx 3.61 \times 10^{-10}$ cm^2/s).[56] To ensure less than a monolayer of water, much lower vacuum pressure is required. Comparison to NEXAFS spectra at lower pressure could potentially elucidate the role of water in the cross-linking mechanism.

The ~536 eV peak is tentatively assigned to ⋝Si–OH, based on peaks reported at 534.4–535.5 eV for various O–H species [i.e., $1s \rightarrow 4\sigma^*$ (O–Si) transition for ⋝Si–OH on the surface of silicon oxide nanowires[57] or OH^- chemisorbed on NaCl (Ref. 58)]. The symbol ⋝represents all the other Si cage or network bonds. To verify peak assignments, NEXAFS spectra were measured for similar compounds with different substituent groups. The spectra for methyl silsesquioxane (MSQ) in its pure, powdered form (PSS-octamethyl substituted, Sigma Aldrich) and solubilized MSQ (polymethylsiloxane in ethanol, Techneglas, Inc.) are shown in Fig. 2. The MSQ is identical to HSQ except that ⋝Si–H groups are replaced by ⋝$Si-CH_3$. In the solubilized MSQ, a small percentage of the ⋝$Si-CH_3$ groups are replaced by ⋝Si–OH.[59] For solubilized MSQ, the NEXAFS line shape is similar to the unexposed HSQ spectrum (Fig. 1), with a sharp peak at 536.7 ± 0.1 eV and a broad peak at 538.7 ± 0.1 eV. However, for pure MSQ (without ⋝Si–OH), the sharper 536.7 eV peak is not observed. This suggests that the 536.7 eV absorption in solubilized MSQ results from the ⋝Si–OH bonds, and that the ~536 eV absorption in unexposed HSQ is likewise due to ⋝Si–OH present in the as-spun film. While there is uncertainty in this assignment due to possible structural differences in these commercially prepared samples, it is consistent with the fact that ⋝Si–OH must also be incorporated into pure HSQ to increase its solubility for spin-on applications.[60,61] The decrease of this ⋝Si–OH associated peak during cross-linking shows that existing ⋝Si–OH groups play an important role in the x-ray induced cross-linking mechanism under these conditions.[2]

The silicon *K*-edge spectra of HSQ [exposed to >0.5 MGy (>17 mJ/cm^2) at 540 eV] shown in Fig. 3 were acquired using the image stack method.[36] With >0.5 MGy x-ray dose, a distinct decrease in the optical density at 1845.4 ± 0.3 eV and an increase at 1847.6 ± 0.3 eV is ob-

Author complimentary copy. Redistribution subject to AIP license or copyright, see http://jvb.aip.org/jvb/copyright.jsp

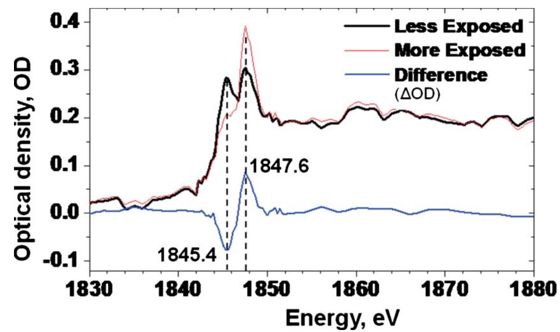

FIG. 3. (Color online) Silicon K-edge NEXAFS spectra of a HSQ thin film, indicating an increase in SiO_2-like structure but no loss of total Si content after x-ray exposure. The "more exposed" region received >0.5 MGy at 540 eV prior to imaging, and both spectral regions received <0.5 MGy at the Si edge (1830–1880 eV) during the image stack (approximate doses).

served. The increasing peak at 1847.6 eV is due to an increase in SiO_2-like bonds.[48,62,63] The decreasing absorption at 1845.4 eV is likely due to a decrease in ⩾Si–OH bonds after exposure, based on previous studies of porous silicon[62,64] (SiO_2) and siloxene.[63] Notably, no features at 1838–1840 eV, which would indicate Si–Si bonds,[62] were observed before or after cross-linking at this x-ray dose.

The Si spectral peak positions and intensities before and after x-ray exposure are similar to those of powdered HSQ solids before and after heating at 500 °C.[65] This implies similar network structures for heated versus x-ray exposed HSQ. However, no decrease in silicon is observed in the exposed region, as evidenced by no change in the post-edge absorption. This is in contrast to the proposed thermal bond redistribution mechanism for HSQ cross-linking, which involves the eventual loss of silane gas (SiH_4).[25,66] The x-ray dose used here may be too small to observe changes in Si content. Although the silicon and oxygen spectra are acquired with a different exposure wavelength and dose, they demonstrate that x-ray induced chemical changes affect the chemical bonding of both silicon and oxygen, as expected for polymer network formation.

B. X-ray induced reaction rate

To quantify x-ray exposure sensitivity and quantitatively relate contrast [ΔOD, Eq. (2)] to cross-linking, HSQ films patterned at increasing dose were imaged at 536 eV and are shown in Fig. 4(a). The contrast at each pixel quantifies the relative degree of cross-linking in the exposed versus unexposed areas, and the sensitivity is defined as the increase in contrast per unit of absorbed x-ray dose. (These definitions of latent contrast and sensitivity are different from, but analogous to, those used in lithography based on developer effects.[1]) Equal-sized features ($1\times5\ \mu m^2$) are exposed at 536 eV in a prebaked HSQ film (500 ± 50 nm thick). The step size is 200 nm, features are separated by 1 μm, and the dwell time is increased exponentially for each subsequent feature (doses from 2.0 ± 0.4 to 276 ± 57 MGy). The patterned area is subsequently imaged at 536 eV, and the x-ray transmission through each feature is shown in Fig. 4(a).

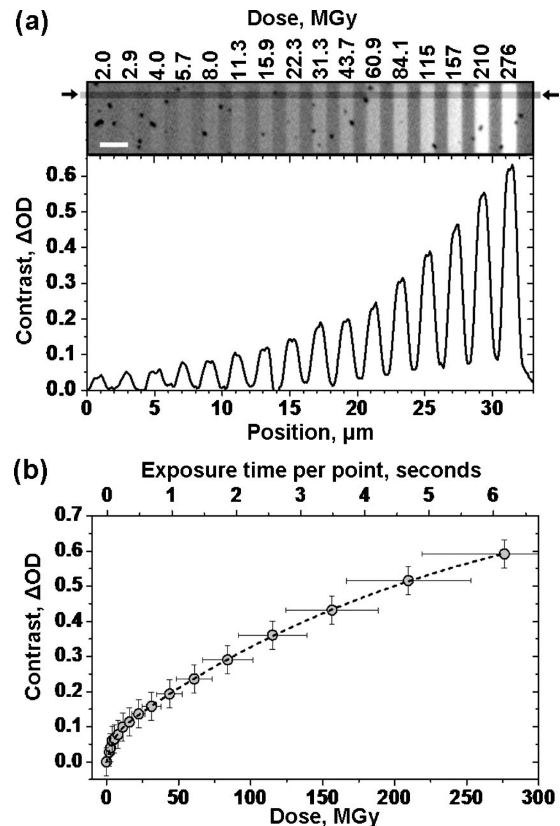

FIG. 4. Dose dependence of x-ray cross-linking in an undeveloped HSQ film. (a) Equally sized features exposed with increasing x-ray dose: STXM image (transmission) and line profile (ΔOD) at oxygen K-edge (536 eV). Lighter regions indicate more transmission and higher degree of cross-linking; dark points are clusters of nanoparticles used for focusing. Line profile is the average contrast through the narrow region indicated by the gray bar and arrows. Scale bar=2 μm. (b) Total average contrast (excluding nanoparticles) vs x-ray dose, indicating two stages of cross-linking and a maximum possible contrast of ΔOD≈0.85. Horizontal error bars are for the MGy axis only.

(Black spots are clusters of 100 nm gold nanoparticles used for focusing.) The line profile indicates the average contrast through the shaded region (highlighted by bold arrows). The contrast values in Fig. 4(b) are averaged across the central 80% of each feature, excluding any nanoparticles. Individual exposed points are not observed within each feature due to spreading of the cross-linking reaction beyond the 50 nm exposure beam width, which is detailed in the following section.

The contrast between exposed and unexposed regions, plotted versus dose and dwell time in Fig. 4(b), shows a sublinear increase in cross-linking with dose. The dashed line fit is $\Delta OD=0.85-0.067\exp(-a/4.2)-0.782\exp(-a/247)$, where a is dose in MGy; this is recast to $\Delta OD=0.85-0.067\exp(-t/0.09)-0.782\exp(-t/5.5)$, where t is exposure time per point in seconds. This double exponential fit indicates a cross-linking process with a fast initial step ($\tau_1=0.09\pm0.01$ s) and a slower second stage ($\tau_2=5.5\pm0.3$ s). These time constants depend on the rate of energy absorption, or absorbed dose rate, just as other reaction rates depend on temperature or laser power. Here the

Author complimentary copy. Redistribution subject to AIP license or copyright, see http://jvb.aip.org/jvb/copyright.jsp

incident flux of ~1.6×10^6 photons/s corresponds to a dose rate of ~42 MGy/s. The fit indicates that cross-linking can continue beyond the highest dose used (276 ± 57 MGy, $19\,339\pm3203$ mJ/cm^2) to a maximum contrast of ΔOD ≈0.85 for fully cross-linked material. Assuming that ΔOD from 0 to 0.85 corresponds to a change from zero to 100% for the relative degree of cross-linking, then ΔOD=0.1, for example, corresponds to an 11.8 ± 4.2% increase in the degree of cross-linking. A linear fit of the lowest-dose points in Fig. 4(b) gives an initial sensitivity of 1.1 ± 0.4% cross-linking increase per MGy x-ray dose, while the highest-dose points yield 0.19 ± 0.07% per MGy. Thus, the initial, fast cross-linking corresponds to higher sensitivity, and the slower cross-linking is equivalent to lower sensitivity.

Evidence for the two-stage mechanism was also observed in near-IR multiphoton-induced cross-linking of HSQ, with slower cross-linking reaction rates ($\tau_1=30\pm10$ s and $\tau_2=3\pm1$ min),[28] presumably due to a lower dose rate and/or different mechanism. One explanation for the two stages could be that photolytically generated reactive sites in close proximity react quite readily. Then, during polymer network formation, the film becomes increasingly rigid, further restricting the mobility of the remaining reactive sites, resulting in a decrease in the rate. Within the solid film, sites with more favorable kinetics for cross-linking due to juxtaposition or angular geometry may cross-link first, and the reaction becomes slower as these sites are consumed.

C. Area-dependent sensitivity

In Fig. 4(a) an increasing "background" level of cross-linking between adjacent features starting at 22.3 MGy (1563 mJ/cm^2, position ~16 μm) is seen. This indicates polymer cross-linking outside the exposed region, consistent with previous STXM and Fourier transform infrared imaging of latent HSQ e-beam patterns.[16,67] Contrast depends on the direct overlap between exposed points based on the beam profile[15] and on the contribution to cross-linking by reaction spread (beyond each exposed point). Thus, this spread could result in the area-dependent sensitivity,[4,15] where obtaining an equivalent peak degree of cross-linking (a requirement for some lithography applications[1,4]) requires a smaller dose for larger features.

To examine how lateral reaction spread contributes to area-dependent sensitivity, a set of features with different widths are patterned at a constant dose. Figure 5(a) shows an unbaked HSQ film (400 ± 50 nm thick) exposed to 8.6 ± 1.4 MGy (484 ± 44 mJ/cm^2) and subsequently imaged at 536 eV. The first feature on the left results from a single-pass line exposure of the x-ray beam at 580 eV with 50 nm step size. Proceeding to the right, the exposed feature width increases to 1.5 μm (produced by 30 adjacent single-pass lines separated by 50 nm). Figure 5(b) plots the increase in peak contrast versus exposed feature width [from Fig. 5(a)]. A small increase in contrast is expected with feature width [lower black curve, Fig. 5(b)], based on the slight overlap between adjacent point exposures. However, the data display a much stronger area dependence. Furthermore, the

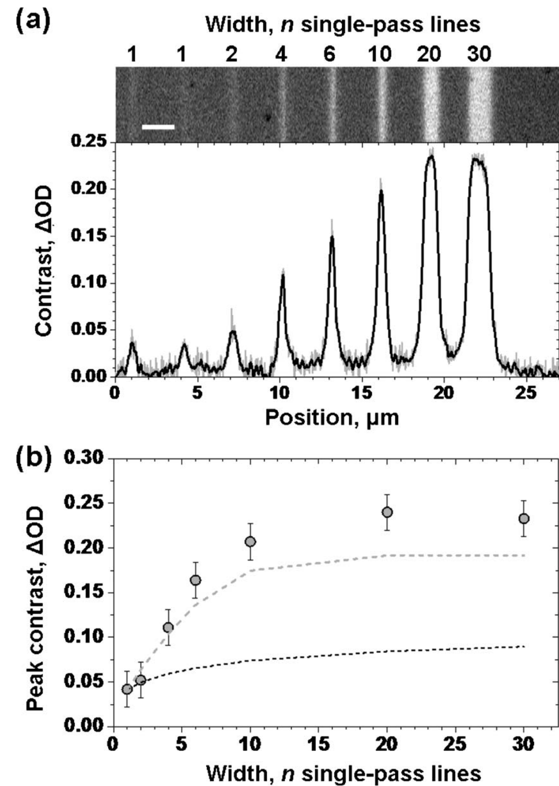

FIG. 5. Area-dependent sensitivity in x-ray cross-linking of HSQ. (a) Increasing size features patterned at constant x-ray dose (8.6 MGy, 536 eV): STXM image (transmission) and line profile (ΔOD) at oxygen *K*-edge (536 eV). Scale bars=2 μm. (b) Peak contrast values from the image above. Lower dashed line (black) is the expected contrast based on the actual exposed area. Upper curve (gray) is simulated using a single-pass line width of 360 nm, as measured. Thus, the peak degree of cross-linking increases with feature width due to spreading effects.

single-pass line exposures in Fig. 5(a) (far left) have an average FWHM of 360 ± 50 nm, which corresponds to a lateral spread of at least 150 nm from the edges of the exposure beam. Therefore, a simulation using a 360 nm FWHM beam profile [upper gray curve, Fig. 5(b)] nearly matches the observed measurements. [The simulated curves in Fig. 5(b) are for isolated features using a 50 nm step size, x-ray beam profile with 50 or 360 nm FWHM, 8.6 MGy dose, and empirical HSQ dose sensitivity from Fig. 4(b).]

Since the step size (50 nm) is much smaller than the reaction spread (150 nm), adjacent points overlap extensively with previously cross-linked material, and cross-linking accumulates to a larger degree than anticipated based only on the absorbed dose. As a result, the peak contrast increases with increasing feature size despite a constant absorbed dose. As shown in the subsequent section, the full extent of the reaction spread is not apparent after development. This could explain why the area-dose dependence cannot be predicted based only the exposure beam profile and developed line widths. Note that the integrated intensity of the line profiles and simulations show that the total degree of cross-linking is approximately linear with increasing feature width; only the peak contrast is area dependent.

Author complimentary copy. Redistribution subject to AIP license or copyright, see http://jvb.aip.org/jvb/copyright.jsp

Interestingly, for up to ten adjacent single-pass lines, the area dependence of the peak contrast is approximately linear. This is consistent with reports for ultrathin, e-beam patterned, and developed HSQ.[15] However, the area dependence saturates once the feature width exceeds the range of the reaction spread (≥ 10 single-pass lines), as the overlap becomes primarily an edge effect. Thus, the area dependence is determined by the patterned feature dimensions relative to the reaction spread distance. This proximity effect is also extremely important for small features that are closely spaced (see supplementary material in Ref. 41 for additional proximity effect results).

D. Dose versus line width: Quantifying reaction spread

Figure 4 and previous HSQ studies[16,67] reveal that the spatial extent of reaction spread is dose dependent. Quantifying the dose dependence may improve lithographic reproducibility, where the dimensions of developed features depend on the local degree of cross-linking. Therefore, the reaction spread was measured in latent single-pass line exposures (50 nm step size, 580 eV exposure) as a function of dose (0.4–111 MGy) and film thickness (100–400 nm). Figure 6(a) shows the raw x-ray transmission image for a set of lines in a 330 ± 50 nm thick HSQ film. Line profiles are vertically averaged along the full length of each line to obtain the FWHM.

For comparison, Fig. 6(b) is a SEM image of this set of lines [from Fig. 6(a)] after room temperature development in 1% NaOH+4% NaCl. Figure 6(c) shows the STXM transmission at 536 eV of the developed lines and the line contrast profiles in OD. The single-pass lines exposed at low doses (0.6 ± 0.3 and 2.1 ± 0.6 MGy) are removed by the developer, while the lines at 3.9 ± 1.0 MGy are just visible. Following the typical definition of onset dose (D_i, the minimum dose required for cross-linked resist to be insoluble during development), this corresponds to an onset dose of $\sim 3.9 \pm 1.0$ MGy or 181 ± 37 mJ/cm^2. This is in agreement, within uncertainty, with the onset dose reported for x-ray lithography in 300 nm thick HSQ films of $D_i \approx 200$ mJ/cm^2 (in TMAOH developer).[30] The dashed line in Fig. 6(a) at a ΔOD of 0.06 ± 0.02 corresponds to the threshold in latent contrast below which all materials are removed by the developer. Based on Fig. 4(b), this threshold level of cross-linking for development contrast (ΔOD=0.06) corresponds to an increase in cross-linking of just 7.1 ± 2.5% of the possible (initial) cross-linkable sites. The initial degree of HSQ cross-linking in the as-spun film (and thus the number of cross-linkable sites) depends on preparation and handling prior to exposure.[12–14,24,68]

Figure 7(a) shows the FWHM of all the latent single-pass lines. Each data point is the mean of two to five independent lines, confirming that the spread in cross-linking increases with dose.[15] For example, in the 330 nm thick film, the latent line width averages 193 ± 40 nm FWHM at the lowest dose (0.6 ± 0.5 MGy), up to 355 ± 7 nm at the highest dose (111 ± 29 MGy), corresponding to a spread of 70–150 nm on either side of the exposure beam profile at the FWHM. Initially, the line width increases sharply with dose, then the rate of increase slows at higher doses. This could indicate a maximum range for the diffusing species or chain reaction and is also consistent with the two-stage cross-linking process described in Sec. III B.

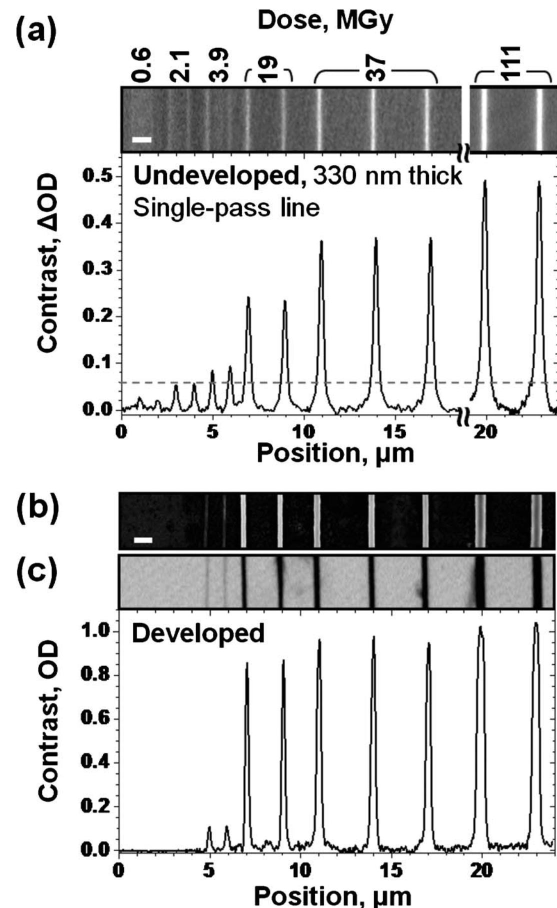

FIG. 6. (a) Single-pass line at increasing dose used to quantify the extent of reaction diffusion: STXM image (transmission) and line profile (ΔOD) at oxygen *K*-edge (536 eV). All cross-linked materials below the dashed line (ΔOD=0.06) are washed away by subsequent development, as shown in (b) SEM image and (c) STXM image at 536 eV (transmission intensity and line profile in OD) of these same lines after development. The developer onset occurs at 3.9 MGy. Scale bars=1 μm.

The reaction spread also increases with film thickness. For the ~ 300 nm thick films, the minimum possible latent line width is 157 ± 5 nm, compared to 190 ± 7 nm for the ~ 330 nm thick films and 223 ± 27 nm for the ~ 400 nm thick films. These values are determined by extrapolating the low dose points to zero dose. Additionally, 90 ± 14 nm wide lines (7.1 ± 2.4 MGy, 100 ± 32 mJ/cm^2) were measured in a developed, 100 ± 20 nm thick HSQ film [Fig. 7(b)]. This figure shows that the trend of narrower lines in thinner samples continues beyond the minimum film thickness accessible by latent STXM imaging. This increase in line width with film thickness is also consistent with recently published results for very thin, developed HSQ.[15,69] One possible ex-

Author complimentary copy. Redistribution subject to AIP license or copyright, see http://jvb.aip.org/jvb/copyright.jsp

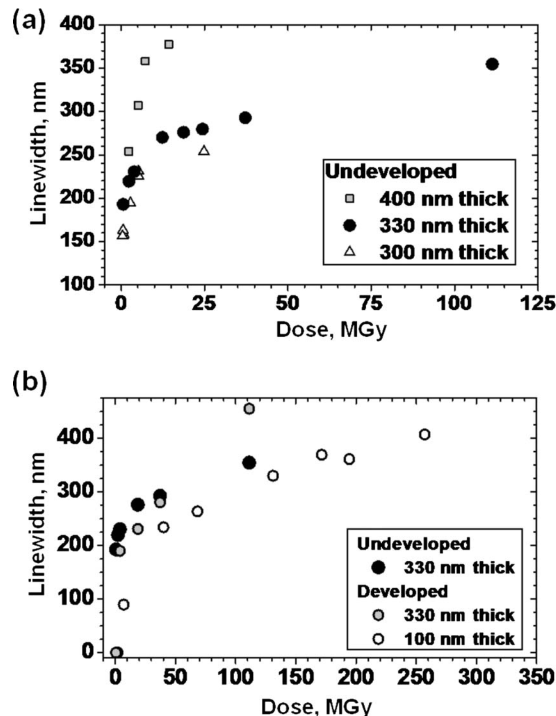

FIG. 7. (a) Plot of undeveloped single-pass line widths, FWHM, showing a strong dependence of width on both dose and film thickness. (b) Plot comparing developed and undeveloped widths, showing similar but slightly sharper lines after development at low doses, due to removal of partially cross-linked material below the threshold [Fig. 6(a), ΔOD=0.06]. SEM measurements of developed lines in 100 nm thick films are considerably narrower, continuing the trend of narrower lines in thinner films.

planation for increased reaction spread with film thickness is that the spread mechanism is inhibited by the surface of the film.

Figure 7(b) shows that single-pass lines are narrower after development at low doses (versus latent image), while at high doses ($\geq$111 MGy) the developed lines are ~30% wider. However, comparing line profiles in Figs. 6(a) and 6(c) reveals that all lines are narrower at their "base" after development, regardless of dose. This is because below the critical cross-linking degree (ΔOD < 0.06), all materials are removed by the developer. This narrowing of the lines is expected based on studies of the developer activity,[70] but detailed line profiles of the undeveloped material were not accessible in that work. Importantly, although cross-linked material below the threshold is removed by the developer, it still contributes to area dependence and other proximity effects.

These lines are substantially wider than in recent state-of-the-art HSQ lithography (4.5–20 nm line width[1,3,21]) due to the film thickness, 50 nm FWHM exposure beam, and delay effects.[13] Preliminary results suggest that the reaction spread—and resulting latent line width and proximity effects—increases significantly with delay between spin-coating and exposure in unbaked films. This line width increase with delay is consistent with previous reports in prebaked and developed HSQ thin films,[14] where the magnitudes of delay effects exceeded stock solution aging effects.[13,14] The area, dose, and thickness dependent effects observed here are consistent with trends in ultrathin HSQ e-beam and photolithography.[1]

E. Potential cause of cross-linking reaction spread

In this work, the reaction spread in latent HSQ patterns was quantified. Since the x-ray beam position is interferometer controlled to better than 10 nm and tightly focused, and we have measured and accounted for the low-dose sensitivity, exposure effects leading to line broadening are ruled out. One possible cause for the >70 nm lateral spread is reactive species diffusing through the film. Reaction spread within this range (100–200 nm) was recently reported in x-ray patterning of thin (~40 nm) positive-tone photoresists [polymethyl methacrylate (PMMA) and polyacrylonitrilie (PAN)]. The results are tentatively attributed to the propagation of radicals and/or ions through the film, but the mechanism has yet to be determined.[44] In that report, it was estimated that heating of the films is negligible (on the order of 5×10^{-4} K), so thermal damage is an unlikely mechanism for the reaction spread.

When a soft x-ray photon at 536–580 eV is absorbed by the HSQ thin film, it excites a core electron in the sample, which decays to produce a high energy Auger electron (~500 eV) and a singly or doubly ionized valence excited state, which can lead to the breaking of nearby bonds at a range of a few nanometers. This produces reactive radical and/or ion fragments and secondary electrons, which can further propagate the reaction.[44] The mean free path of scattered 0–580 eV electrons in HSQ should be similar to amorphous glass and polymers of similar density (<10 nm).[71,72] The effect of low energy secondary electrons (10–50 eV) in e-beam lithography of HSQ is limited to a range of ~2 nm.[73] Therefore, we suspect that small radicals or ions are responsible for the >70 nm reaction spread through the film. A variety of mechanisms could explain the reaction spread, including reactions of protons or H radicals liberated by the cleavage of the ⋟Si–H bonds during x-ray absorption. These may propagate some distance before reacting and initiating cross-linking, possibly leading to a chain reaction. See supplementary material in Ref. 41 for detailed reaction mechanisms. Both H atom and proton initiated mechanisms could account for the decrease in ⋟Si–OH (silanol) and increase in oxygen with cross-linking observed in the NEXAFS spectra in this study.

IV. SUMMARY AND CONCLUSIONS

Direct-write x-ray lithography and subsequent x-ray imaging of latent photoresist patterns is a powerful way to monitor the chemistry of x-ray induced processes in the absence of developer effects. Oxygen and silicon edge NEXAFS spectra of HSQ films before and after x-ray exposure show that the total oxygen content in x-ray exposed regions increases while the ⋟Si–OH content decreases, and no change in silicon content is observed. This indicates the incorporation of existing ⋟Si–OH into the network and an uptake of water and/or additional oxygen in cross-linked re-

Author complimentary copy. Redistribution subject to AIP license or copyright, see http://jvb.aip.org/jvb/copyright.jsp

gions. The sensitivity of HSQ cross-linking to direct x-ray exposure reveals that the cross-linking proceeds by a rapid initial step ($\tau_1 = 0.09 \pm 0.01$ s) followed by a slower second stage ($\tau_2 = 5.5 \pm 0.3$ s), suggesting that an initial number of easily cross-linked sites are consumed quickly, producing a more rigid network, which resists further cross-linking. Thus, a higher absolute degree of cross-linking reduces the sensitivity of HSQ films. The developer solution removes material below a critical, relative cross-linking degree of $7.1 \pm 2.5\%$ (relative to the maximum number of available cross-linkable sites), whether it is cross-linked by direct exposure or reaction spread.

A dose and thickness dependent reaction front spread of 70–150 nm is revealed in these HSQ films, independent of developer conditions. The full extent of this spread is not apparent after high-contrast, room-temperature development. However, it is crucial to understanding the resolution-limiting characteristics of HSQ and correcting for proximity effects to obtain well-defined final feature dimensions. The long range and thickness dependence of this reaction spread may be due to the diffusion of H atoms or protons through the HSQ film. STXM imaging requires >250 nm thick HSQ films for good signal-to-noise ratios, but the chemical information, line width versus thickness trends, and their relation to proximity effects appear to be applicable for thinner films as well.

Future work on HSQ should address the role of water and ⩾Si–OH in the cross-linking mechanism and determine whether H radical or proton diffusion is responsible for the reaction spread. Interestingly, HSQ is the resist used to fabricate the next generation of Fresnel zone plates currently in development (12–15 nm outer diameter),[5] so higher resolution x-ray lithography and STXM imaging are made possible in part by a better understanding of HSQ chemistry. Furthermore, with a better understanding of the cross-linking mechanism, delay effects, and the cause of reaction spread, new and better photoresists based on HSQ can be designed to fabricate the next generation of smaller, faster, more reliable electronic devices and new nanoscale optical devices.

ACKNOWLEDGMENTS

The authors sincerely thank Deirdre L. Olynick, Monika Fleischer, Adam Leontowich, Adam P. Hitchcock, and T. Don Tilley for the discussion of HSQ lithography and mechanisms. They also thank A. L. David Kilcoyne for many hours of support in designing the STXM experiments, Chris J. Hahn for SEM measurements, and Stefan Pastine for the discussion of mechanisms and chemicals for inhibitor experiments. Salary support was provided by the Chemical Sciences Division (M.K.G. and S.R.L.), Laboratory Directed Research and Development (A.G.C.), and the Material Sciences Division (A.G.C. and A.V.T.) of Lawrence Berkeley National Laboratory. These divisions, as well as the Advanced Light Source, were supported by the Director, Office of Science, Office of Basic Energy Sciences, U.S. Department of Energy, under Contract No. DE-AC02-05CH11231. X-ray materials research and S.K.'s salary were supported by the NSF ERC for Extreme Ultraviolet Science and Technology (Contract No. EEC-0310717) and the Alexander von Humboldt Foundation.

[1] A. E. Grigorescu and C. W. Hagen, Nanotechnology **20**, 292001 (2009).
[2] H. Namatsu, Y. Takahashi, K. Yamazaki, T. Yamaguchi, M. Nagase, and K. Kurihara, J. Vac. Sci. Technol. B **16**, 69 (1998).
[3] J. K. W. Yang, B. Cord, H. G. Duan, K. K. Berggren, J. Klingfus, S. W. Nam, K. B. Kim, and M. J. Rooks, J. Vac. Sci. Technol. B **27**, 2622 (2009).
[4] J. A. Liddle, F. Salmassi, P. P. Naulleau, and E. M. Gullikson, J. Vac. Sci. Technol. B **21**, 2980 (2003).
[5] W. L. Chao, J. Kim, S. Rekawa, P. Fischer, and E. Anderson, J. Vac. Sci. Technol. B **27**, 2606 (2009).
[6] D. Gil, R. J. Menon, and H. I. Smith, J. Vac. Sci. Technol. B **21**, 2956 (2003).
[7] D. L. Olynick, B. D. Harteneck, E. Veklerov, M. Tendulkar, J. A. Liddle, A. L. D. Kilcoyne, and T. Tyliszczak, J. Vac. Sci. Technol. B **22**, 3186 (2004).
[8] F. Stade, A. Heeren, M. Fleischer, and D. P. Kern, Microelectron. Eng. **84**, 1589 (2007).
[9] M. Guillorn *et al.*, J. Vac. Sci. Technol. B **27**, 2588 (2009).
[10] K. Keil, K. H. Choi, C. Hohle, J. Kretz, L. Szikszai, and J. W. Bartha, J. Vac. Sci. Technol. B **27**, 47 (2009).
[11] A. E. Grigorescu, M. C. Van der Krogt, and C. W. Hagen, J. Micro/Nanolith. MEMS MOEMS **6**, 043006 (2007).
[12] M. Häffner, A. Haug, A. Heeren, M. Fleischer, H. Peisert, T. Chassé, and D. P. Kern, J. Vac. Sci. Technol. B **25**, 2045 (2007).
[13] F. C. M. J. M. van Delft, J. Vac. Sci. Technol. B **20**, 2932 (2002).
[14] N. Clark, A. Vanderslice, R. Grove, and R. R. Krchnavek, J. Vac. Sci. Technol. B **24**, 3073 (2006).
[15] A. E. Grigorescu, M. C. van der Krogt, C. W. Hagen, and P. Kruit, J. Vac. Sci. Technol. B **25**, 1998 (2007).
[16] D. L. Olynick, J. A. Liddle, A. V. Tivanski, M. K. Gilles, T. Tyliszczak, F. Salmassi, K. Liang, and S. R. Leone, J. Vac. Sci. Technol. B **24**, 3048 (2006).
[17] D. L. Olynick, B. Cord, A. Schipotinin, D. F. Ogletree, and P. J. Schuck, J. Vac. Sci. Technol. B **28**, 581 (2010).
[18] A. E. Grigorescu, M. C. van der Krogt, C. W. Hagen, and P. Kruit, Microelectron. Eng. **84**, 822 (2007).
[19] Y. Ekinci, H. H. Solak, C. Padeste, J. Gobrecht, M. P. Stoykovich, and P. F. Nealey, Microelectron. Eng. **84**, 700 (2007).
[20] T. C. Chang, T. M. Tsai, P. T. Liu, Y. S. Mor, C. W. Chen, J. T. Sheu, and T. Y. Tsengb, Electrochem. Solid-State Lett. **6**, G69 (2003).
[21] X. L. Zhu, C. Q. Xie, M. H. Zhang, M. Liu, B. Q. Chen, and F. Pan, Chin. Phys. Lett. **26**, 086803 (2009).
[22] D. Tilley University of California, Berkeley, CA (private communication).
[23] P. T. Liu, T. C. Chang, T. M. Tsai, Z. W. Lin, C. W. Chen, B. C. Chen, and S. M. Sze, Appl. Phys. Lett. **83**, 4226 (2003).
[24] M. J. Loboda, C. M. Grove, and R. F. Schneider, J. Electrochem. Soc. **145**, 2861 (1998).
[25] Y. K. Siew, G. Sarkar, X. Hu, J. Hui, A. See, and C. T. Chua, J. Electrochem. Soc. **147**, 335 (2000).
[26] J. A. van Kan, F. Zhang, C. Zhang, A. A. Bettiol, and F. Watt, Nucl. Instrum. Methods Phys. Res. B **266**, 1676 (2008).
[27] V. Sidorkin, E. van Veldhoven, E. van der Drift, P. Alkemade, H. Salemink, and D. Maas, J. Vac. Sci. Technol. B **27**, L18 (2009).
[28] A. G. Caster, S. Kowarik, A. M. Schwartzberg, O. Nicolet, S. H. Lim, and S. R. Leone, J. Raman Spectrosc. **40**, 770 (2009).
[29] A. G. Caster, S. Kowarik, and S. R. Leone (unpublished).
[30] I. P. Junarsa and P. F. Nealey, J. Vac. Sci. Technol. B **22**, 2685 (2004).
[31] I. P. Junarsa, M. P. Stoykovich, P. F. Nealey, Y. Ma, F. Cerrina, and H. H. Solak, J. Vac. Sci. Technol. B **23**, 138 (2005).
[32] M. Peuker, M. H. Lim, H. I. Smith, R. Morton, A. K. van Langen-Suurling, J. Romijn, E. W. J. M. van der Drift, and F. C. M. J. M van Delft, Microelectron. Eng. **61–62**, 803 (2002).
[33] Y. F. Chen, H. F. Yang, and Z. Cui, Microelectron. Eng. **83**, 1119 (2006).
[34] S. Choi, N. Jin, V. Kumar, I. Adesida, and M. Shannon, J. Vac. Sci. Technol. B **25**, 2085 (2007).
[35] L. Muntean, R. Planques, A. L. D. Kilcoyne, S. R. Leone, M. K. Gilles,

Author complimentary copy. Redistribution subject to AIP license or copyright, see http://jvb.aip.org/jvb/copyright.jsp

and W. D. Hinsberg, J. Vac. Sci. Technol. B **23**, 1630 (2005).
[36]A. L. D. Kilcoyne *et al.*, J. Synchrotron Radiat. **10**, 125 (2003).
[37]T. Tyliszczak *et al.*, AIP Conf. Proc. **705**, 1356 (2004).
[38]J. Wang, Ph.D. thesis, McMaster University, 2008.
[39]D. Attwood, *Soft X-Rays and Extreme Ultraviolet Radiation: Principles and Applications* (Cambridge University Press, New York, NY, 1999), p. 360–361.
[40]J. M. Heck, D. Attwood, W. Meyer-Ilse, and E. H. Anderson, J. X-Ray Sci. Technol. **8**, 95 (1998).
[41]See supplementary material at http://dx.doi.org/10.1116/1.3514124 for exposure patterns, proximity effect data and detailed reaction mechanisms.
[42]A. L. D. Kilcoyne, Lawrence Berkeley National Laboratory, Berkeley, CA (private communication).
[43]J. N. Bremmer, Y. Liu, K. G. Gruszynski, and F. C. Dali, Mater. Res. Soc. Symp. Proc. **476**, 37 (1997).
[44]J. Wang, H. D. H. Stover, A. P. Hitchcock, and T. Tyliszczak, J. Synchrotron Radiat. **14**, 181 (2007).
[45]At. Data Nucl. Data Tables **55**, 349 (1993).
[46]E. M. Gullikson, X-Ray Interactions with Matter, http://www.cxro.msd.lbl.gov/
[47]J. K. W. Yang and K. K. Berggren, J. Vac. Sci. Technol. B **25**, 2025 (2007).
[48]I. Tanaka, J. Kawai, and H. Adachi, Phys. Rev. B **52**, 11733 (1995).
[49]G. E. Brown, Jr., G. A. Waychunas, J. Stohr, and F. Sette, J. Phys. Colloq. **47**, C8-685 (1986).
[50]J. Stohr, *NEXAFS Spectroscopy*, Springer Series in Surface Sciences, edited by G. Ertl, R. Gomer, D. L. Mills, and H. K. V. Lotsch (Springer-Verlag, Berlin, 1992), Vol. 25, p. 93–95.
[51]R. A. Bubeck, P. R. Dvornic, J. Hu, A. Hexemer, X. Li, S. E. Keinath, and D. A. Fischer, Macromol. Chem. Phys. **206**, 1146 (2005).
[52]D. Coulman, A. Puschmann, U. Hofer, H. P. Steinruck, W. Wurth, P. Feulner, and D. Menzel, J. Chem. Phys. **93**, 58 (1990).
[53]N. Pangher, A. Schmalz, and J. Haase, Chem. Phys. Lett. **221**, 189 (1994).
[54]Y. Daiko, T. Kasuga, and M. Nogami, Microporous Mesoporous Mater. **69**, 149 (2004).
[55]C. C. Yang and W. C. Chen, J. Mater. Chem. **12**, 1138 (2002).
[56]J. H. Zhao, I. Malik, T. Ryan, E. T. Ogawa, and P. S. Ho, Appl. Phys. Lett. **74**, 944 (1999).
[57]L. W. Lin, Y. H. Tang, X. X. Li, L. Z. Pei, Y. Zhange, and C. Guo, J. Appl. Phys. **101**, 014314 (2007).
[58]U. Malaske, H. Pfnur, M. Bassler, M. Weiss, and E. Umbach, Phys. Rev. B **53**, 13115 (1996).
[59]Techneglas, Inc., Perrysburg, OH (private communication).
[60]G. Dubois, IBM Almaden Research Center, San Jose, CA (private communication).
[61]M. Fleischer, Molecular Foundry, Lawrence Berkeley National Laboratory, Berkeley, CA (private communication).
[62]S. C. Bayliss, Q. Zhang, and D. A. Hutt, Phys. Status Solidi B **190**, 85 (1995).
[63]S. L. Friedman, M. A. Marcus, D. L. Adler, Y.-H. Xie, T. D. Harris, and P. H. Citrin, Mater. Res. Soc. Symp. Proc. **298**, 295 (1993).
[64]S. C. Bayliss, P. Anstee, D. A. Hutt, Q. Zhang, N. Danson, J. Bates, and A. Waddilove, J. Appl. Phys. **76**, 5171 (1994).
[65]C. M. Hessel, E. J. Henderson, J. A. Kelly, R. G. Cavell, T. K. Sham, and J. G. C. Veinot, J. Phys. Chem. C **112**, 14247 (2008).
[66]V. Belot, R. Corriu, D. Leclercq, P. H. Mutin, and A. Vioux, Chem. Mater. **3**, 127 (1991).
[67]A. Tivanski, D. L. Olynick, M. K. Gilles, and S. R. Leone (unpublished).
[68]W. C. Liu, C. C. Yang, W. C. Chen, B. T. Dai, and M. S. Tsai, J. Non-Cryst. Solids **311**, 233 (2002).
[69]V. Sidorkin, A. E. Grigorescu, H. Salemink, and E. van der Drift, Microelectron. Eng. **86**, 749 (2009).
[70]S. W. Nam, M. J. Rooks, J. K. W. Yang, K. K. Berggren, H. M. Kim, M. H. Lee, K. B. Kim, J. H. Sim, and D. Y. Yoon, J. Vac. Sci. Technol. B **27**, 2635 (2009).
[71]C. W. Lee, Y. Ikematsu, and D. Shindo, J. Electron Microsc. **51**, 143 (2002).
[72]S. Tanuma, C. J. Powell, and D. R. Penn, Surf. Interface Anal. **21**, 165 (1994).
[73]K. Yamazaki and H. Namatsu, Jpn. J. Appl. Phys., Part 1 **43**, 3767 (2004).

Author complimentary copy. Redistribution subject to AIP license or copyright, see http://jvb.aip.org/jvb/copyright.jsp